

OBSERVATIONS OF THE NICKEL LAYER IN THE MESOPAUSE REGION AT MID-LATITUDES

Michael Gerding¹, Kathrin Baumgarten¹, John M. C. Plane²

¹Leibniz-Institute of Atmospheric Physics at the Rostock University, 18225 Kuehlungsborn, Germany

²School of Chemistry, University of Leeds, Leeds LS2 9JT, United Kingdom

*Email: gerding@iap-kborn.de

ABSTRACT

Observations of the mesospheric Ni layer have been performed by lidar in January-March 2018 at Kuehlungsborn/Germany (54°N, 12°E). These soundings provide only the second Ni data set after initial observations by Collins et al. at Chatanika/Alaska (65°N, 147°W)^[1]. We utilized for the first time a transition from the low-lying excited Ni(³D) state at 341 nm. For all soundings, nightly mean peak densities varied between ~280 cm⁻³ and 450 cm⁻³, which is a factor of ~40 less than previously reported for Chatanika^[1]. The observed Ni abundance is especially important if compared with the abundance of other metals like Fe, and with their respective abundances in evaporating meteoroids, which form the source of the metal layer in the upper mesosphere. Here, we present exemplarily a sounding from January 8, 2018. Beside the Ni raw data and density profiles we show a temperature profile as measured simultaneously by the co-located RMR lidar and the temperature variation due to gravity waves and tides.

1. INTRODUCTION

Ablation of meteoroids entering the Earth's atmosphere forms a metal layer between ~80 and 110 km. This layer has been detected first 90 years ago by Na airglow observations^[2]. Nowadays, ground-based lidars are used for quantitative studies, and more species have been detected subsequently (e.g., Fe, K, Ca, Ca⁺, Li)^[3-7]. It turned out quickly that the abundances of the different species do not resemble the ratios found in typical meteoroids^[8,9]. Lidar observations of the metal concentrations as well as measurements of chemical reaction rates and modelling of meteoroid heating revealed a complex interplay of different factors determining the height-dependent concentrations of the particular metal atoms^[10]. Hence, any additional metal species provides new

independent information to deepen our knowledge about the middle atmospheric dynamics and chemistry.

Collins et al. described first Ni observations from Chatanika/Alaska^[1]. During two lidar soundings, they observed peak densities of ~16,000 cm⁻³ and a total abundance of 2.7 x 10⁻¹⁰ cm⁻², which is about 0.8 times the typical Fe abundance at this site. This Ni abundance is surprisingly large compared to the Fe/Ni ratio of ~18 in CI-Chondrites^[8]. The observation of Ni by lidar and other methods is generally technically challenging because of the small resonance backscatter cross section and the short UV wavelength. We have been able to observe the mesospheric Ni layer by lidar during six nights between January and March 2018 at Kuehlungsborn/Germany (54.1°N, 11.7°E). First results are already published in *Geophys. Res. Lett.*^[11], hereafter cited as GDP2019. Here, we present additional technical information about the soundings. Additionally we show two examples of one-hour mean profiles from a single night. Simultaneous soundings with a co-located RMR lidar provided independent temperature observations and allowed to deduce information about activity of gravity and tidal waves for that night.

2. METHODOLOGY

The Ni lidar observations at Kuehlungsborn have been made with a dye laser system pumped by an excimer laser at 308 nm^[6]. The dye laser has been tuned to the resonance wavelength of the Ni(³D) state at $\lambda_{\text{air}} = 341.4764$ nm. (For additional soundings we also tuned the laser to the Ni(³F) resonance $\lambda_{\text{air}} = 336.9563$ nm, but for clarity we concentrate here on the description of the first case. More information on advantages and disadvantages of the different resonance transitions is provided in GDP2019.) With two amplifier stages, we got a laser pulse energy of ~14 mJ. The

bandwidth of the laser was limited to 0.4 pm by an intra-cavity etalon. The backscattered photons are collected by a 78-cm telescope and detected by a Hamamatsu R7600-200 photomultiplier. For background suppression we used an interference filter with 29 nm bandwidth (full width at half maximum) and $\sim 85\%$ transmission. The comparatively large bandwidth allowed to detect all relevant backscatter wavelengths, but limited the observations to moonless nights.

Fig. 1 shows the differential backscatter cross section σ_{diff} of the Ni(^3D) resonance line, the laser spectrum and the correspondent effective differential backscatter cross section σ_{eff} . Ni densities at altitude z are calculated by the equation

$$\rho_{\text{Ni}}(z) = \rho_{\text{air}}(z_R) \cdot \sigma_{\text{Ray}} / \sigma_{\text{eff}} \cdot N_{\text{res}}^{\text{corr}}(z) / N_{\text{Ray}}^{\text{corr}}(z_R) \cdot P$$

with $\sigma_{\text{eff}} = 1.08 \times 10^{-17} \text{ m}^2/\text{sr}$ and $\sigma_{\text{Ray}} = 3.57 \times 10^{-31} \text{ m}^2/\text{sr}$, $N_{\text{c,res}}$ and $N_{\text{c,Ray}}$ range-corrected resonance and Rayleigh count rate and $\rho_{\text{air}}(z_R)$ air density at reference altitude z_R , taken from NRLMSISE-00 [12]. An additional factor P accounts for the thermal population of the Ni(^3D) state of $\sim 15\%$ at typical temperatures of 200 K around 90 km altitude.

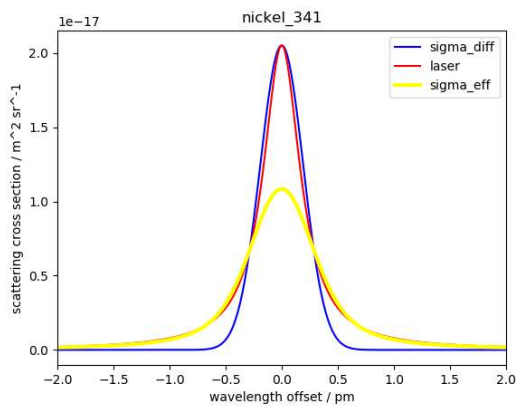


Fig. 1: Blue: Differential backscatter cross section for excitation of the low-lying excited Ni(^3D) state. Red: Approximated laser spectrum (Lorentz-shape). Yellow: Effective differential backscatter cross section (convolution of laser and σ_{diff}).

Simultaneous soundings with the co-located RMR lidar [13] can be used to check the focusing of the beam widening optics and the overlap with the telescope. Fig. 2 shows the background-corrected backscatter at 341 nm together with the count rate

of the RMR lidar 532 nm high-altitude channel. At altitudes without Ni resonance backscatter, both profiles perfectly agree, confirming good adjustment of beam widening optics and telescope.

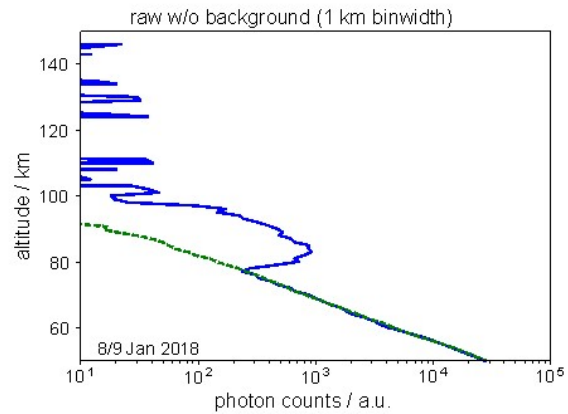


Fig. 2: Background-corrected raw data at 341 nm (blue), integrated 21–22 UTC on Jan. 8, 2018 with 1 km binwidth. The green dashed line is the 532 nm backscatter of the RMR lidar for the same period.

The main purpose of the RMR lidar are temperature soundings in the middle atmosphere. Taking advantage of different optical filtering techniques, we are able to suppress the daylight background efficiently and continue the temperature soundings during day and night [13]. This allows detailed studies of gravity waves as well as tidal waves [14,15].

3. RESULTS

We examined the Ni layer during six moonless nights between January and March 2018. Each sounding lasted between 40 min and 2.5 h. Fig. 3 shows exemplarily two one-hour mean profiles from January 8, 2018 (18:30 – 19:30 UTC, blue, and 21:00 – 22:00 UTC, red). In the beginning of the sounding the Ni layer appeared between 77 km and ~ 100 km with a clear maximum at 84 km. A peak density of $\sim 290 \text{ atoms}/\text{cm}^3$ was observed. The layer shape has changed in the later profile. The layer was getting narrower but showed a broader maximum (or maybe even a double maximum). Peak density decreased to $\sim 240 \text{ atoms}/\text{cm}^3$. Also the column abundance decreased by about 20%, from $3.48 \times 10^{-8} \text{ cm}^{-2}$ to $2.74 \times 10^{-8} \text{ cm}^{-2}$. We will discuss potential reasons for the density change below.

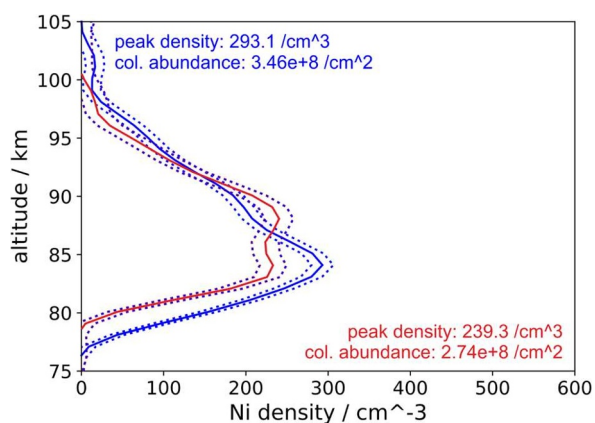


Fig. 3: Ni density profiles for 18:30-19:30 UTC (blue) and 21:00 – 22:00 UTC (red) on Jan. 8, 2018. Bin width is 1 km. The plot is smoothed by a 7-point Hann-filter for visualization only.

Comparing all different nights, we detected Ni mean peak densities between 280 and 450 cm^{-3} . Peak altitudes varied between 83 km and 87 km.

The Ni backscatter cross section is calculated for an ambient temperature of 200 K. Fig. 4 shows that this assumption is valid on average, but that the temperature above 75 km is quite variable due to the presence of gravity waves and tides. The lower mesosphere on Jan 8/9 is slightly warmer than usual and shows prominent large-scale waves. We would like to note that the polar vortex was slightly shifted towards the North-Atlantic and Kuehlungsborn was on its outer edge. Nevertheless, conditions for a Sudden Stratospheric Warming were not fulfilled.

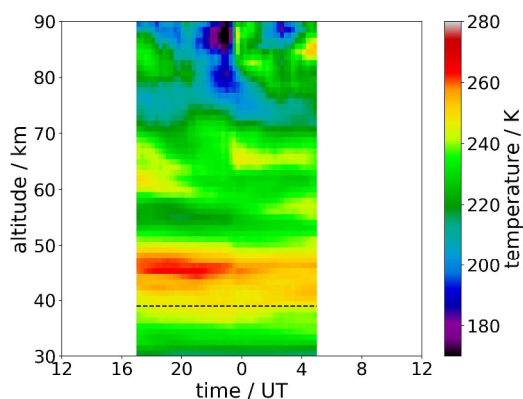


Fig. 4: Temperature observations with the RMR lidar at Kuehlungsborn. Data are limited to nighttime to cover also the upper mesosphere. Integration time is 2 h. The dashed line denotes transition of height channels.

Fig. 5 shows the temperature variability after filtering with a long-pass Butterworth filter (15 km cut-off). The wavelike structures are now most probable due to tides. Please note the amplitudes of at least ± 10 K above 80 km, which add up to the temperature variation by gravity waves. Of course, the short data set, even if extending up to at least 90 km, limits the detectability of tides. Below 73 km this soundings covers nearly 48 h continuously. These results are in general agreement with the nighttime data set (not shown).

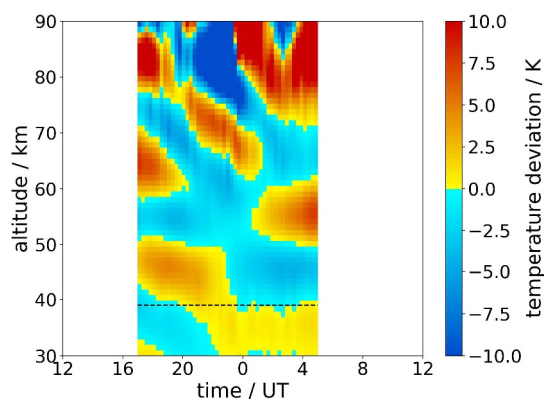


Fig. 5: Temperature variation after filtering with 15 km low-pass Butterworth filter. Waves with these large vertical wavelength are typically attributed to tides.

The temperature variability above 80 km implies some uncertainty on the absolute Ni densities. As mentioned above, the backscatter cross section is calculated for a constant temperature of 200 K, which is a reasonable assumption. We checked the population of the lower Ni state also for 180 and 220 K and found a variation by $\sim 20\%$ (cf. Supporting Information of GDP2019). This is in the order of magnitude of the Ni variation shown above. Therefore, we attribute a large fraction of the observed density change to the systematic uncertainty in the backscatter cross section. We plan to take the temperature-dependence of the backscatter cross section into account in a future study. On the other hand, the large night-to-night variability of the Ni density is hardly an artifact but due to dynamical and chemical effects. Similar variability has been found also with other metals [5-7].

In summary, we were able to observe the second set of Ni observations after initial studies by Collins et al. [1]. We found a similar layer shape, but

a strongly reduces Ni density. Comparing with mid-latitude Fe observations^[16] we got a Fe/Ni ratio of 38, which is within a factor of ~2 of the ratio found in CI-Chondrites (Fe/Ni \approx 18). These data provide an important benchmark for future studies including chemical transport models etc. So far, we do not have an explanation for the different results obtained at Chatanika/Alaska and Kuehlungsborn/Germany. Finally we would like to note that the observations of the Ni(³F) ground-state gave similar results, but a strongly reduced lidar performance. Therefore, we suggest to use the Ni(³D) transition in future.

[15] K. Baumgarten et al., *Atmos. Chem. Phys.*, **18**, 371–384 (2018)

[16] T. J. Kane and C. S. Gardner, *J. Geophys. Res.*, **98**, 16,875-16,886 (1993)

ACKNOWLEDGEMENTS

We thank our colleagues Josef Höffner, Torsten Köpnick, Reik Ostermann and Michael Priester (all IAP) as well as Shane Daly (U Leeds) for their help with installation of the Ni lidar. JMCP acknowledges funding by the Natural Environment Research Council (grant NE/P001815/1).

REFERENCES

- [1] R. Collins et al., *Geophys. Res. Lett.*, **42**, 665–671, doi: 10.1002/2014GL062716 (2015).
- [2] V. M. Slipher, *Publ. Astro. Soc. Pac.*, **41**, 262-265 (1929)
- [3] J. P. Jegou et al., *Geophys. Res. Lett.*, **7**, 995-998 (1980)
- [4] J. Qian and C. S. Gardner, *J. Geophys. Res.*, **100**, 7453-7461 (1995)
- [5] V. Eska et al., *J. Geophys. Res.* **103**, 29,207-29,214 (1998)
- [6] M. Gerding et al., *J. Geophys. Res.*, **105**, 27,131-27,146 (2000)
- [7] X. Chu et al., *Geophys. Res. Lett.*, **38**, L23807 (2011)
- [8] J. M. C. Plane, *Int. Rev. Phys. Chem.*, **10**, 55-106 (1991)
- [9] S. Raizada et al., *J. Atmos. Solar-Terr. Phys.*, **66**, 596-606 (2004)
- [10] J. M. C. Plane et al., *Chem. Rev.*, **115**, 4497-4541 (2015)
- [11] M. Gerding et al., *Geophys. Res. Lett.*, **46**, 408-415, doi: 10.1029/2018GL080701 (2019)
- [12] J. M. Picone et al., *J. Geophys. Res.*, **107**, 1468 (2002)
- [13] M. Gerding et al., *Atmos. Meas. Tech.*, **9**, 3707-3715 (2016)
- [14] M. Kopp et al., *J. Atmos. Solar-Terr. Phys.*, **127**, 37-50 (2015)